IEEE Access
Multidisciplinary ⋮ Rapid Review ⋮ Open Access Journal

Received 21 June 2023, accepted 29 June 2023, date of publication 4 July 2023, date of current version 12 July 2023.

Digital Object Identifier 10.1109/ACCESS.2023.3292265

RESEARCH ARTICLE

Fuzzy Automatic Disturbance Rejection Control of Quadrotor UAV Based on Improved Whale Optimization Algorithm

ZEBIAO SHAN[1,2,3], YUHANG WANG[1], XIAOSONG LIU[1], AND CHANGBIN WEI[1]

[1]School of Electronic and Information Engineering, Changchun University of Science and Technology, Changchun 130022, China
[2]College of Communication Engineering, Jilin University, Changchun 130022, China
[3]Changchun Meteorological Instrument Research Institute, Changchun 130102, China

Corresponding author: Xiaosong Liu (liuxs@cust.edu.cn)

This work was supported in part by the Natural Science Foundation of Jilin Province under Grant No. YDZJ202301ZYTS412. Entitled "Research on parameter estimation method of array signals based on fractional order cumulant".

ABSTRACT With the aim of improving the rapidity and accuracy of quadrotor UAV positional trajectory tracking, this paper proposes a fuzzy automatic disturbance rejection control of quadrotor UAV based on improved whale optimization algorithm (IWOA-Fuzzy-ADRC). (1) To address the problems of low accuracy and slow convergence of the traditional whale algorithm, a combination of logistic chaos mapping and skew tent mapping is applied to improve the diversity of the initial population. (2) The global search capability is strengthened to avoid falling into local optimum through introducing the cross operator and Gaussian variational operators. (3) The IWOA is employed to iteratively optimize the adjustment coefficients of the fuzzy active disturbance rejection controller, the calculus gain of the nonlinear state error feedback control (NLSEF), and the error correction coefficients of the expansive state observer (ESO). The simulation results demonstrate that compared with the traditional ADRC controller and PID controller, the proposed IWOA-Fuzzy-ADRC controller can effectively improve the control performance of the system, accurately track the desired flight trajectory, accelerate the dynamic response of the control system, reduce the steady-state error, and enhance the anti-interference capability.

INDEX TERMS UAV trajectory tracking, fuzzy ADRC, whale optimization algorithm, chaotic mapping, cross-operator, Gaussian variant operators.

I. INTRODUCTION

The quadrotor UAV has a simple structure, good maneuverability, easy operation, does not require a complex steering mechanism to control the cyclic torque of the rotor, and only needs to change the rotational speed of rotor fixed on the motor to complete all flight motions. This has enabled its wide application in agricultural low-altitude spraying, military, logistics delivery, searching and rescue (SAR), and hazardous environment operations, as well as became a research hotspot in recent years [1], [2]. Nevertheless, quadrotor UAV are characterized by nonlinearity, resulting in the system being strongly coupled, underdriven, and susceptible to external disturbances. To address the problems above, Han proposed a nonlinear controller called automatic disturbance rejection control (ADRC) [3], which utilizes a relevant observer to estimate the model uncertainty and external environmental disturbances of system unmodeled in real time. Additionally, the desired control performance is obtained through setting the corresponding control laws. With these strategies, not only the weaknesses existing in the traditional PID control [4] are improved, but also the performance of the control system is greatly enhanced. Wameedh et al. [5] applied a model-free active input-output feedback linearization technique of the modified automatic disturbance rejection control paradigm for a single-link flexible joint manipulator to remove the generalized disturbance of system uncertainty in real time and convert the system to a

The associate editor coordinating the review of this manuscript and approving it for publication was Tiankui Zhang.

chain of integrators. However, the system parameters are too complicated to make them satisfy the system requirements as quickly as possible. Amjad and Hussein [6] utilized linear automatic disturbance rejection control (LADRC) and nonlinear automatic disturbance rejection control (NADRC) to control the position trajectory of a single-link flexible joint robot and used the PSO to adjust the parameters of two controllers for improving the system performance. Nevertheless, the process of encoding weights and selecting genetic operators for the algorithm is too complex. In order to further improve the control performance of controller and realize the online adjustment of controller parameters, numerous scholars introduced the fuzzy rules to control the system (i.e., fuzzy PID control strategy [7] and fuzzy ADRC control strategy [8], [9].). For instance, Tao Liang employed the fuzzy logic rule to adjust the coefficients of extended state observer (ESO) as a way to enhance the robustness of the system against external disturbances and parameter changes [10]. Unfortunately, this method fails to solve the issue of inappropriate parameter selection of the fuzzy controller itself, which results in the control system cannot track external disturbances well and affects the control performance of system.

It is worth noting that the parameters of ESO and nonlinear state error feedback control rate (NLSEF) in ADRC are very important. Nonetheless, the setting process of these parameters is too complex and therefore some optimization algorithms need to be introduced to adjust them (e.g., grey wolf algorithm [11], [12], radial basis neural network algorithm [13], traditional genetic algorithm [14], [15], [16], adaptive genetic algorithm [17], particle swarm algorithm [18]). Recently, Wang Xiaojing exploited the grey wolf algorithm to optimize the controller parameters to improve the controller accuracy, but this algorithm is subject to the convergence factor and tends to fall into a local optimum [19]. Furthermore, Shen and Xu [20] established a state observer via modern control theory, and estimated the unknown total disturbance with an adaptive radial basis function (RBF) neural network, while the gradient descent method employed in RBF is not optimized and therefore suffers from problems such as slow convergence.

Compared to the above algorithms, whale optimization algorithm (WOA) has characteristics of simple operation and few control parameters [21], making it possible to have better optimization capability under high complexity system. For example, CUI Zhizhong exploited WOA to perform online tuning of PI controller and ADRC control parameters [22]. While the weak global search capability and low initial population diversity of conventional WOA algorithm lead to the algorithm easily falling into local optimality and failing to obtain the optimal solution of the problem to be solved.

In this paper, an improved whale optimization algorithm (IWOA) is proposed to adjust the parameters of a fuzzy automatic disturbance rejection control system, and an IWOA-Fuzzy-ADRC controller is designed to accurately track the positional trajectory of a quadrotor UAV. The work in this paper can be summarized as follows:

a) In order to solve the problem of low convergence accuracy and slow convergence speed of the traditional WOA, a combination of logistic chaos mapping and skew tent mapping is developed to improve the initial population diversity.
b) With the aim of preventing the model from falling into local optima in the search process, the crossover operator and Gaussian variational operator are introduced to enhance the global search capability of the model.
c) The IWOA optimization algorithm is obtained by combining (1) and (2), as well as its superiority is demonstrated by comparing it with other optimization algorithms.
d) A novel IWOA-Fuzzy-ADRC controller is designed for position trajectory tracking of a quadrotor UAV. The IWOA is used to iteratively optimize the optimal adjustment coefficients, the calculus gain of the nonlinear state error feedback control rate (NLSEF) in the fuzzy self-rejecting controller and the error correction coefficients of the expansive state observer (ESO).
e) The IWOA-Fuzzy-ADRC controller is compared with the ADRC controller and the PID controller in terms of effectiveness, dynamic performance and stability for tracking the positional trajectory of a quadrotor UAV.

II. DYNAMICS MODEL OF THE QUADROTOR UAV

The quadrotor UAV is a flight system consisting of a frame arranged in a cross or X-shape and four motor-connected fixed rotors, which can carry various sensors for detecting attitude information [23], [24].

The quadrotor UAV system is modelled under the assumptions that: (1) the quadrotor UAV is a rigid body with constant mass and inertia moment; (2) the gravity center is constant and coincides with the geometric center of the body; and (3) the UAV is subject to only gravity and the pull of the propeller. The Newton-Euler principle is implemented to model the quadrotor UAV system, neglecting the air resistance. The nonlinear model of the quadrotor UAV is:

$$\begin{cases} \ddot{\phi} = \dfrac{I_y - I_z}{I_x}\dot{\theta}\dot{\psi} + \dfrac{L}{I_x}U_2 - Lk_\phi\dot{\phi} + \Delta_\phi \\ \ddot{\theta} = \dfrac{I_z - I_x}{I_y}\dot{\phi}\dot{\psi} + \dfrac{L}{I_y}U_3 - Lk_\theta\dot{\theta} + \Delta_\theta \\ \ddot{\psi} = \dfrac{I_x - I_y}{I_z}\dot{\phi}\dot{\theta} + \dfrac{1}{I_z}U_4 - k_\psi\dot{\psi} + \Delta_\psi \\ \ddot{x} = \dfrac{U_1}{m}(\sin\theta\cos\phi\cos\psi + \sin\phi\sin\psi) - k_x\dot{x} + \Delta_x \\ \ddot{y} = \dfrac{U_1}{m}(\sin\theta\cos\phi\sin\psi - \sin\phi\cos\psi) - k_y\dot{y} + \Delta_y \\ \ddot{z} = \dfrac{U_1}{m}\cos\theta\cos\phi - g - k_z\dot{z} + \Delta_z \end{cases} \tag{1}$$

where ϕ, θ and ψ are the cross-roll, pitch and yaw angles of the quadrotor UAV respectively; L is the distance from the rotor center to the origin of the body coordinate; x, y and z are the positions of the UAV in the three directions respectively; m is the mass of the UAV; I_x, I_y and I_z are the rotational inertia of the UAV; g is the acceleration of gravity; $k_x, k_y, k_z, k_\theta, k_\psi$ and k_ϕ are the drag coefficients of each channel; $\Delta_x, \Delta_y, \Delta_z \Delta_\theta, \Delta_\psi$ and Δ_ϕ are the bounded interference or unmodelled parts respectively; and U_1, U_2, U_3 and U_4 are four control inputs of the system.

$$\begin{cases} U_1 = k_1(\omega_1^2 + \omega_2^2 + \omega_3^2 + \omega_4^2) \\ U_2 = k_1(-\omega_2^2 + \omega_4^2) \\ U_3 = k_1(-\omega_1^2 + \omega_3^2) \\ U_4 = k_2(\omega_1^2 - \omega_2^2 + \omega_3^2 - \omega_4^2) \end{cases} \tag{2}$$

where k_1 and k_2 represent the lift and drag coefficients of a rotor; as well as $\omega_1, \omega_2, \omega_3$ and ω_4 are the rotational speeds of four motors respectively.

Since the model of a quadrotor UAV has a strong nonlinear character, it is not conducive to the controller design. Therefore, in order to reduce the complexity of controller design, the model of a quadrotor UAV is linearized according to the minimum angle assumption:

$$\begin{cases} \ddot{\phi} = \dfrac{1}{I_x} U_2 \\ \ddot{\theta} = \dfrac{1}{I_y} U_3 \\ \ddot{\psi} = \dfrac{1}{I_z} U_4 \\ \ddot{x} = -g\theta \\ \ddot{y} = g\phi \\ \ddot{z} = -\dfrac{U_1}{m} + g \end{cases} \tag{3}$$

It can be seen that the linearized model not only reduces the non-linear characteristic of the system, but also simplifies the coupling relationship between position and attitude, reducing the complexity of the control system design. The framework of a quadrotor UAV control system obtained from the linearized model is shown in FIG. 1.

In the control process of a quadrotor UAV, the position controller in the x and y directions calculates the desired pitch and roll angles respectively based on the input reference signals x_{ref} and y_{ref}; the roll angle controller and the pitch angle controller calculate the inputs U_2 and U_3 respectively based on the desired attitude obtained from the position controller; while for the position controller and the yaw angle controller in the z direction, both can calculate the inputs U_1 and U_4 respectively directly based on the input reference position z_{ref} and desired yaw angle ψ_{ref}.Then, the actual position and attitude of the UAV can be obtained from the calculated inputs and feed them back into the system, creating a double closed-loop structure.

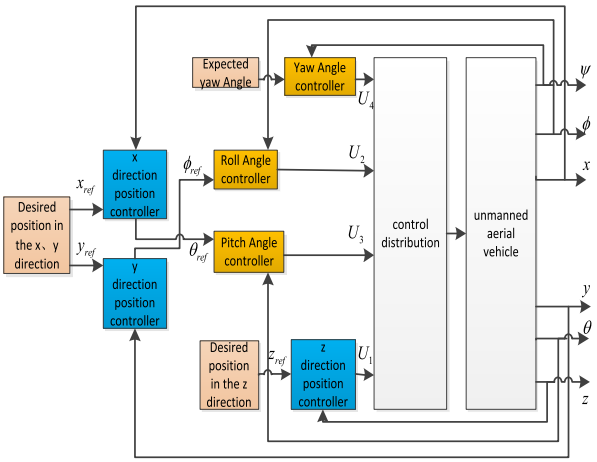

FIGURE 1. Controller structure of quadrotor UAV.

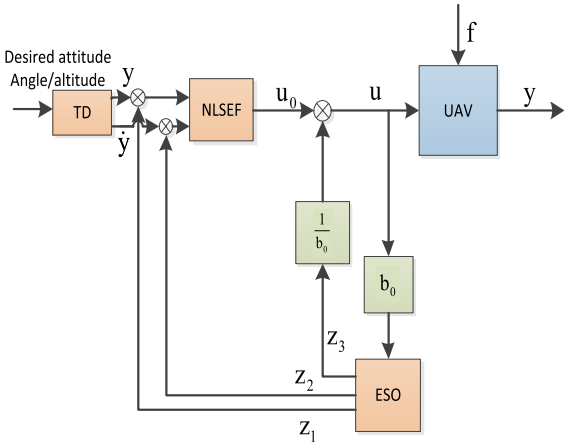

FIGURE 2. The structure of ADRC control system.

III. FUZZY ADRC CONTROLLER

Conventional ADRC is mainly composed of an extended state observer (ESO), a tracking differentiator (TD) and a nonlinear state error feedback control (NLSEF). Firstly, the error between the input and output of system is obtained. Then, the over-processing process is arranged for the given signal with non-linear TD to obtain the values of required differential components. Finally, the weighted sum is converted to a nonlinear form by NLSEF, the expansion state observer ESO detects the total disturbance, the disturbance is estimated and the actual control signal of system is gained. In order to enable the quadrotor UAV control system to estimate and compensate for uncertain disturbances accurately in real time, this paper improves the ADRC controller by introducing a fuzzy controller and an IWOA for achieving parameter self-tuning. The structure of the ADRC control system is shown in FIG. 2.

A. TRACKING DIFFERENTIATOR

TD consists of two inertial segments connected in parallel to complete the transition process in the control process. The effect of transitioning the input is achieved by continuously tracking the input via a first-order delay segment and deriving its approximate differentiation. Furthermore, the problem of overshooting during regulation is avoided by arranging the transition process of system. The discrete form of TD is as follows:

$$\begin{cases} x_1(k+1) = x_1(k) + hx_2(k) \\ x_2(k+1) = x_2(k) + hfhan \\ f_{han} = -rsign(x_1(k) - v(k) + \dfrac{(x_2(k)|x_2(k)|)}{2r}) \end{cases} \tag{4}$$

where f_{han} is a second-order discrete function designed to solve the problem that the system cannot reach the desired value in finite time and stops at the desired value, the specific expression of which is:

$$u = f_{han}(x_1, x_2, r, h)$$
$$\begin{cases} d = rh \\ d_0 = hd \\ y = x_1 + hx_2 \\ a_0 = \sqrt{d^2 + 8r|y|} \\ a = \begin{cases} x_1 + 0.5(a_0 - d)sign(y) & |y| > d_0 \\ x_2 + y/h & |y| \le d_0 \end{cases} \\ f_{han} = -\begin{cases} rsign(a) & |a| > d \\ r\frac{a}{d} & |a| \le d \end{cases} \end{cases} \tag{5}$$

where x_1 is the system's expected value $v(k)$ of tracking signal; x_2 is the differential of the system's tracking signal; h is the integration step of the function that determines the effect of the system's noise filtering; and r determines how fast the system tracks the input signal.

B. NONLINEAR STATE ERROR FEEDBACK CONTROL

NLSEF utilizes the deviation of each state quantity of system in a form of non-linear combination (i.e., the actual control value of system obtained by a non-linear combination of the difference between the actual value and estimated value observed by ESO) to constitute the output, thus improving the control performance of system, and can flexibly match the relationship between the proportion and differentiation of error to achieve the good control effect. The mathematical expression is illustrated as:

$$\begin{cases} e_1 = v_1 - z_1 \\ e_2 = v_2 - z_2 \\ u_0 = \beta_1 fal(e_1, \alpha_1, \delta) + \beta_2 fal(e_2, \alpha_2, \delta) \\ fal(e, \alpha, \delta) = \begin{cases} \frac{e}{\delta^{\alpha-1}} & |e| \le \delta \\ |e|^{\alpha} sign(e) & |e| > \delta \end{cases} \end{cases} \tag{6}$$

where v_1 and v_2 are the tracking input of nonlinear error feedback rate and its differentiation, respectively; z_1 and z_2 represent the deviation output of each ESO state; u_0 is the control quantity formed by a certain nonlinear combination of NLSEF; β_1 and β_2 are the gains of integration and differentiation in NLSEF, respectively; $fal(e, \alpha, \delta)$ is the nonlinear function, where δ denotes the range of linear segment lengths.

C. EXTENDED STATE OBSERVER

As the disturbance affects the system output, we consider the external disturbance as a new state of controlled system and construct the ESO estimating new variables via feedback, which is not dependent on the specific mathematical model generating disturbance and requires no direct measurement of action. For common second-order systems, the discrete expression for ESO is:

$$\begin{cases} e(k) = z_1(k) - y(k) \\ z_1(k+1) = z_1(k) + h[z_2(k) - \beta_{01} fal(e_1, \alpha_1, \delta)] \\ z_2(k+1) = z_2(k) + h[z_3(k) - \beta_{02} fal(e_1, \alpha_2, \delta) + bu] \\ z_3(k+1) = z_3(k) + h\beta_{03} fal(e, \alpha_3, \delta) \end{cases} \tag{7}$$

where $\beta_{0i}(i = 1, 2, 3)$ is the output error gain; δ is the length of linear interval; $fal(e, \alpha_i, \delta)(i = 1, 2, 3)$ is a non-linear function used to suppress signal jitter with the expression:

$$fal(e_1, \alpha_i, \delta) = \begin{cases} \dfrac{e}{\delta^{1-\alpha_i}} & |e_1| \le \delta \\ |e_1|^{\alpha_i} sign(e_1) & |e_1| > \delta \end{cases} \tag{8}$$

where δ is the length of linear interval for function fal; b is the compensation factor that determines the compensation strength, generally taken as 1; and $\beta_{0i}(i = 1, 2, 3)$ is the output error gain.

D. IWOA-BASED FUZZY ADRC CONTROLLER

Taking the quadrotor UAV channel x as an example, we present the fuzzy ADRC controller for channel x and construct other channels in the same way.

We utilize the IWOA algorithm to obtain the optimal adjustment coefficients $kbetai\_x(i = 1, 2)$ and $kbeta0i\_x(i = 1, 2, 3)$ for the fuzzy ADRC controller and to optimize β_1, β_2 and $\beta_{0i}(i = 1, 2, 3)$ simultaneously. The difference between the desired and actual values is taken as the input of fuzzy control, after the selection of affiliation function and the determination of fuzzy rules, and after the defuzzification, two signals $dbeta\_x$ and $dbeta0\_x$ are output, which are finally used as the adjustment amount of β_1, β_2 and $\beta_{0i}(i = 1, 2, 3)$, so that the parameters can be self-tuned and the control effect of system can be improved.

$$\begin{cases} beta1\_x' = beta1\_x + kbeta1\_x^* dbeta\_x \\ beta2\_x' = beta2\_x + kbeta2\_x^* dbeta\_x \end{cases} \tag{9}$$

where $betai\_x'(i = 1, 2)$ is the parameter β_1 and β_2 in the NLSEF optimized by the fuzzy control and IWOA algorithm; $betai\_x(i = 1, 2)$ is the βi $(i = 1, 2)$ optimized by the IWOA

algorithm; and $kbetai\_x * dbeta\_x\,(i = 1, 2)$ is the adjustment amount of fuzzy control output.

The parameter $\beta_{0i}(i = 1, 2, 3)$ in the ESO after fuzzy control and optimization via IWOA algorithm can be expressed as:

$$\begin{cases} beta01\_x' = beta01\_x + kbeta01\_x^{*}dbeta0\_x \\ beta02\_x' = beta02\_x + kbeta02\_x^{*}dbeta0\_x \\ beta03\_x' = beta03\_x + kbeta03\_x^{*}dbeta0\_x \end{cases} \tag{10}$$

where $beta0i\_x'(i = 1, 2, 3)$ indicates the parameter $\beta_{0i}(i = 1, 2, 3)$ in the ESO after optimization by fuzzy control and IWOA; $beta0i\_x$ $(i = 1, 2, 3)$ is $\beta_{0i}(i = 1, 2, 3)$ after optimization by IWOA; $kbeta0i\_x * dbeta0\_x\,(i = 1, 2, 3)$ is the adjustment amount of fuzzy control output. The structure of proposed IWOA-Fuzzy-ADRC is illustrated in FIG.3.

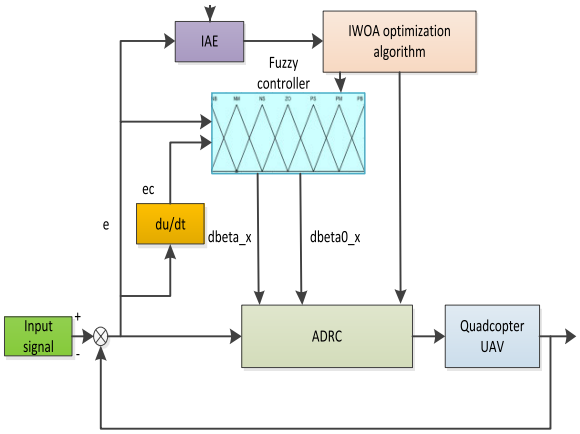

FIGURE 3. Controller structure of IWOA-Fuzzy-ADRC.

In fuzzy control, ''trimf'' is selected as the affiliation function in this paper. *dbeta_x* and *dbeta0_x* fuzzy rules are listed in Tables 1-2.

TABLE 1. ***dbeta_x*** **Fuzzy control rule table.**

dbeta_x		ec						
		NB	NM	NS	ZO	PS	PM	PB
	NB	PB	PB	PM	PM	PS	ZO	ZO
	NM	PB	PB	PM	PM	PS	ZO	ZO
	NS	PM	PM	PS	PS	PS	PS	NS
e	ZO	PM	PS	PS	NB	PM	NB	NS
	PS	NS	NS	NS	NS	PM	NM	NM
	PM	PM	PM	PB	PB	PB	PB	PB
	PB	PB	PB	PB	PB	PB	PB	PB

E. ANALYSIS OF CONTROLLER STABILITY

In this paper, the controller stability is investigated with the roll angle ϕ as an example. From the dynamics model of system, it is clear that the quadrotor UAV is a typical underdriven

TABLE 2. ***dbeta0_x*** **Fuzzy control rule table.**

dbeta0_x		ec						
		NB	NM	NS	ZO	PS	PM	PB
	NB	PB	PB	PM	PM	PS	ZO	ZO
	NM	PB	PB	PM	PM	PS	ZO	ZO
	NS	PM	PM	PS	PS	ZO	ZO	NS
e	ZO	PM	PS	PS	ZO	NS	NS	NM
	PS	PS	ZO	ZO	NS	NM	NM	NM
	PM	ZO	ZO	NS	NM	NM	NB	NB
	PB	ZO	NS	NM	NM	NB	NB	NB

system with the following equations of attitude subsystem:

$$\begin{cases} \ddot{\phi} = \dfrac{I_y - I_z}{I_x}\dot{\theta}\dot{\psi} + \dfrac{L}{I_x}U_2 - Lk_\phi\dot{\phi} + \Delta_\phi \\ \ddot{\theta} = \dfrac{I_z - I_x}{I_y}\dot{\phi}\dot{\psi} + \dfrac{L}{I_y}U_3 - Lk_\theta\dot{\theta} + \Delta_\theta \\ \ddot{\psi} = \dfrac{I_x - I_y}{I_z}\dot{\phi}\dot{\theta} + \dfrac{1}{I_z}U_4 - k_\psi\dot{\psi} + \Delta_\psi \end{cases} \tag{11}$$

which can be obtained by organizing:

$$\begin{bmatrix} \ddot{\phi} \\ \ddot{\theta} \\ \ddot{\psi} \end{bmatrix} = \begin{bmatrix} f_1(\phi, \theta, \psi, \omega) \\ f_2(\phi, \theta, \psi, \omega) \\ f_3(\phi, \theta, \psi, \omega) \end{bmatrix} + B\begin{bmatrix} U_2 \\ U_3 \\ U_4 \end{bmatrix} \tag{12}$$

where $B = \begin{bmatrix} L/I_x & 0 & 0 \\ 0 & L/I_y & 0 \\ 0 & 0 & L/I_z \end{bmatrix}$;

$$\begin{cases} f_1 = \frac{I_y - I_z}{I_x}\dot{\theta}\dot{\psi} - Lk_\phi\dot{\phi} + \Delta_\phi \\ f_2 = \frac{I_z - I_x}{I_y}\dot{\phi}\dot{\psi} - Lk_\theta\dot{\theta} + \Delta_\theta \\ f_3 = \frac{I_x - I_y}{I_z}\dot{\phi}\dot{\theta} - k_\psi\dot{\psi} + \Delta_\psi \end{cases} \tag{13}$$

Let $\xi_1 = \phi, \xi_2 = \dot{\phi}$ and $\xi_3 = f_1$, and assuming $\dot{f}_1 = h$ and bounded, $\xi = \begin{bmatrix} \xi_1 & \xi_2 & \xi_3 \end{bmatrix}^T$. The equation for the roll angle is expressed in the form of a state quantity equation as follows:

$$\begin{cases} \dot{\xi} = A\xi + BU_2 + Eh \\ \phi = C\xi \end{cases} \tag{14}$$

where $A = \begin{bmatrix} 0 & 1 & 0 \\ 0 & 0 & 1 \\ 0 & 0 & 0 \end{bmatrix}$, $B = \begin{bmatrix} 0 \\ L/I_x \\ 0 \end{bmatrix}$, $C = \begin{bmatrix} 1 \\ 0 \\ 0 \end{bmatrix}^T$ and $E = \begin{bmatrix} 0 & 0 & 1 \end{bmatrix}^T$.

For analysis simplicity, the poles of the configuration observer are all located at $-\omega_0$, then the characteristic polynomial $\lambda(s)$ can be expressed as:

$$\lambda(s) = s^3 + 3\omega_0 s^2 + 3\omega_0^2 s + \omega_0^3 = (s + \omega_0)^3 \tag{15}$$

in which ω_0 is the bandwidth of the observer. The larger the bandwidth of the observer, the more accurate the estimate will be, but an excessive bandwidth will increase the sensitivity to noise. The gain of the observer can be expressed $Q = \begin{bmatrix} 3\omega_0 & 3\omega_0^2 & \omega_0{}^3 \end{bmatrix}$.

Let $\tilde{\xi}_i = \xi_i - \hat{\xi}_i (i = 1, 2, 3)$, the state equation for estimation error of the state observer is established according

to Eq. (14):

$$\begin{cases} \dot{\tilde{\xi}}_1 = \tilde{\xi}_2 - q_1\tilde{\xi}_1 \\ \dot{\tilde{\xi}}_2 = \tilde{\xi}_3 - q_2\tilde{\xi}_1 \\ \dot{\tilde{\xi}}_3 = h - q_3\tilde{\xi}_1 \end{cases} \tag{16}$$

Let $\varepsilon_i = (\tilde{\xi}_i)/(\omega_0^{i-1})(i = 1, 2, 3)$, then Eq. (16) can be changed to

$$\dot{\varepsilon} = \omega_0 A_\varepsilon \varepsilon + \frac{B_\varepsilon}{\omega_0^2} h \tag{17}$$

where $A_\varepsilon = \begin{bmatrix} -3 & 1 & 0 \\ -3 & 0 & 1 \\ -1 & 0 & 0 \end{bmatrix}$ and $B_\varepsilon = \begin{bmatrix} 0 \\ 0 \\ 1 \end{bmatrix}$.

Theorem 1: Since h is bounded, there exists a constant $\sigma_i > 0$ as well as time $T_i > 0$. If $t \geq T_i$ exists and $\omega_0 > 0$, then $|\tilde{\xi}_i| \leq \sigma_i(i = 1, 2, 3)$ and thus the estimation error is bounded for bounded inputs to the system, i.e., the closed-loop system is asymptotically stable.

Proof: The solution to Eq. (17) is:

$$\varepsilon(t) = e^{\omega_0 A_\varepsilon t}\varepsilon(0) + \int_0^t e^{\omega_0 A_\varepsilon (t-\tau)} \frac{B_\varepsilon}{\omega_0^2} h d\tau \tag{18}$$

Let $H(t) = \int_0^t e^{\omega_0 A_\varepsilon (t-\tau)} \frac{B_\varepsilon}{\omega_0^2} h d\tau$, h is bounded, i.e., there exists a positive number μ,making $|h| \leq \mu$, then:

$$|H_i(t)| \leq \frac{\mu}{\omega_0^3}\left[|(A_\varepsilon^{-1}B_\varepsilon)_i| + |(A_\varepsilon^{-1}B_\varepsilon e^{\omega_0 A_\varepsilon t})_i|\right] \tag{19}$$

where $|(A_\varepsilon^{-1}B_\varepsilon)_i| = \begin{cases} 1|_{i=1} \\ 3|_{i=2,3} \end{cases}$.

Since the triple pole configuration of ESO is at $-\omega_0$, then A_ε is Hurwitz stable, and for $t \geq T_i > 0$ with $|(e^{\omega_0 A_\varepsilon t}B_\varepsilon)_i| \leq \frac{1}{\omega_0^3}(i = 1, 2, 3)$ i.e.,

$$|(A_\varepsilon^{-1}e^{\omega_0 A_\varepsilon t}B_\varepsilon)_i| \leq \begin{cases} \frac{1}{\omega_0^3}|_{i=1} \\ \frac{4}{\omega_0^3}|_{i=2,3} \end{cases} \tag{20}$$

thereby obtaining $|H_i(t)| \leq \frac{3\mu}{\omega_0^3} + \frac{4\mu}{\omega_0^6}(i = 1, 2, 3)$.

Assuming $\varepsilon_s(0) = |\varepsilon_1(0)| + |\varepsilon_2(0)| + |\varepsilon_3(0)|$, the same is obtained:

$$|[e^{\omega_0 A_\varepsilon t}\varepsilon(0)]_i| \leq \frac{\varepsilon_s(0)}{\omega_0^3} \tag{21}$$

From Eq. (18), it can be obtained that:

$$|\varepsilon_i(t)| \leq |[e^{\omega_0 A_\varepsilon t}\varepsilon(0)]_i| + |H_i(t)| \tag{22}$$

Suppose that $\tilde{\xi}_s(0) = |\tilde{\xi}_1(0)| + |\tilde{\xi}_2(0)| + |\tilde{\xi}_3(0)|$, due to $\varepsilon_i = (\tilde{\xi}_i)/(\omega_0^{i-1})(i = 1, 2, 3)$, combined with (18), (19) and (21), for all $t \geq T_i > 0$, which can be obtained as follows:

$$\tilde{\xi}_i(t) \leq |\frac{\tilde{\xi}_s(0)}{\omega_0^3}| + \frac{3\mu}{\omega_0^{4-i}} + \frac{4\mu}{\omega_0^{7-i}} = \sigma_i \tag{23}$$

where, $i = 1, 2, 3$. Proof of completion.

In order to ensure that the designed fuzzy controller is stable, the input/output (I/O) stability theory is used for the analysis. According to the I/O stability theorem, sufficient conditions for system stability are obtained by proving that the system transfer function and the fuzzy feedback controller are obtuse and strictly obtuse, respectively [25].

The roll angle equation transfer function is obtained from Eq. (14) as:

$$G(s) = \frac{1}{\frac{I_x}{L}s^2 + I_x k_\varphi s} \tag{24}$$

From the obtuseness theorem, it can be seen that the controlled object $G(s)$ is not originally obtuse. For the controlled object and the controller multiplied by $(s + n)$ and $(s + n)^{-1}$, respectively, the transfer functions of the transformed equivalent control object and feedback controller are:

$$G'(s) = \frac{s + n}{\frac{I_x}{L}s^2 + I_x k_\varphi s} \tag{25}$$

$$G_c'(s) = \frac{1}{s + n}(\beta_1 + \beta_2 s) \tag{26}$$

If $Re(G'(j\omega)) \geq 0$ is satisfied, then $G'(s)$ is obtuse, so there is:

$$\begin{aligned} Re(G'(j\omega)) &= Re\left[\frac{(j\omega + n)(\frac{I_x}{L}(j\omega)^2 - I_x k_\varphi j\omega)}{(\frac{I_x}{L})^2(j\omega)^4 - (I_x k_\varphi)^2(j\omega)^2}\right] \\ &= Re\left[\frac{-\frac{I_x n}{L}\omega^2 + I_x k_\varphi \omega^2 - \frac{I_x}{L}(j\omega)^3 - I_x k_\varphi n(j\omega)}{(\frac{I_x}{L})^2\omega^4 + (I_x k_\varphi)^2\omega^2}\right] \\ &= \frac{-\frac{I_x n}{L} + I_x k_\varphi}{(\frac{I_x}{L})^2\omega^2 + (I_x k_\varphi)^2} \end{aligned} \tag{27}$$

When $k_\varphi L \geq n$, then $Re(G'(j\omega)) \geq 0$ and $G'(s)$ are obtuse. If $Re(G_c'(j\omega)) \geq \mu$ (where $\mu > 0$) is satisfied, then $G'(s)$ is strictly obtuse, so there is:

$$\begin{aligned} Re(G_c'(j\omega)) &= Re\left[\frac{(\beta_1 + \beta_2 s)(n - s)}{(s + n)(n - s)}\right] \\ &= Re\left[\frac{\beta_1 n + \beta_2\omega^2 - \beta_1 s + \beta_2 n s}{n^2 + \omega^2}\right] \\ &= \frac{\beta_1 n + \beta_2\omega^2}{n^2 + \omega^2} \end{aligned} \tag{28}$$

If $\beta_1 n > 0$, $\beta_2 \geq 0$, then $Re(G_c'(j\omega)) \geq \mu$ and $G'(s)$ are strictly obtuse.

Thus, it can be shown that the roll angle controller satisfies the sufficient conditions for I/O stability as follows:

$$k_\varphi L \geq n, \beta_1 n > 0, \beta_2 \geq 0 \tag{29}$$

Similarly, it can be deduced that other directions satisfy the I/O stability sufficiency condition.

IV. WHALE OPTIMIZATION ALGORITHM

A. CONVENTIONAL WOA

With the advantages of simple operation and few control parameters [26], the WOA simulates the hunting behavior of humpback whales consisting of three main stages: encircling prey, bubble net hunting and searching for prey.

1) ENCIRCLING PREY

Since the location of the optimal individual (prey) is unknown in the search space, the WOA assumes that the current best candidate solution (i.e., the solution with the lowest fitness value) is the location of target prey or the closest prey. Other individuals update their positions towards the optimal solution with the following expressions:

$$D = |C \cdot X^*(t) - X(t)| \tag{30}$$

$$X(t+1) = X^*(t) - A \cdot D \tag{31}$$

in which t is the current number of iterations; X^* denotes the position vector of the current best solution; X represents the position vector of the individual whale; D indicates the distance between the individual whale and its prey; $||$ is the absolute value; $\cdot$ means the element-by-element multiplication; as well as A and C are coefficient vectors for the way whales swim, with the following expressions:

$$A = 2a \cdot r - a \tag{32}$$

$$C = 2 \cdot r \tag{33}$$

$$a = 2 - \frac{2t}{T_{\max}} \tag{34}$$

where r is a random vector in interval [0, 1]; a denotes a control parameter that decreases linearly from 2 to 0 with the number of iterations; and $T_{\max}$ indicates the maximum number of iterations.

2) BUBBLE NET HUNTING

The bubble net attack consists of two main mechanisms: shrinkage bracketing and spiral update position. The shrink bracketing mechanism is described as decreasing the value of a in Eq. (32) from 2 to 0 during the iterative process, with A fluctuating in the interval $[-a, a]$ at this point. When A is a random value within the interval $[-1, 1]$, the whale can approach from the original position to target position and perform a shrinking bracket. The spiral update position mechanism first calculates the distance from individual whale (X, Y) to prey (X^*, Y^*), and then models the spiral motion of humpback whales with a spiral equation, which is expressed as follows:

$$X(t+1) = D \cdot e^{bl} \cdot \cos(2\pi l) + X^*(t) \tag{35}$$

where D is the distance from the individual whale to its prey, i.e., $D = |X^*(t) - X(t)|$; b denotes a constant defining the logarithmic spiral shape; and l is a random number within the interval $[-1, 1]$.

Suppose that humpback whales perform shrinkage bracketing and spiral update position with a one-half probability, the mathematical model is described as follows:

$$X(t+1) = \begin{cases} X^*(t) - A \cdot Dp < 0.5 \\ D \cdot e^{bl} \cdot \cos(2\pi l) + X^*(t) \quad p \geq 0.5 \end{cases} \tag{36}$$

where p is the random number in interval [0, 1].

3) SEARCHING FOR PREY

When $|A| \geq 1$, the whale population performs the global search and no longer updates its position based on the current optimal solution, but updates its position based on a randomly selected whale to find the optimal solution for population diversity, with the following expressions:

$$D_{rand} = |C \cdot X_{rand}(t) - X(t)| \tag{37}$$

$$X(t+1) = X_{rand}(t) - D_{rand} \tag{38}$$

where X_{rand} denotes the position vector of the randomly selected whale individual from the whale population; and D_{rand} indicates the distance between the randomly selected whale individual and its prey.

B. CHAOTIC SEQUENCES-BASED WOA

WOA searches for optimal solutions based mainly on probability and spiral update position mechanism. Nevertheless, as the initial populations are basically randomly initialized in the search space, resulting in the overall probability distribution is not uniform and mainly limited to few small intervals for local search, which cannot effectively extract all information in the space. For this reason, the initial population should be distributed over the whole search space as much as possible to shorten the redundancy time of the algorithm in global search stage, and thus search for the location of optimal solutions rapidly.

Chaos is the non-linear behavior with characteristics such as regularity and randomness, where the Logistic mapping chaotic sequence is able to undergo all states without repetition in a certain range, the mathematical expression is:

$$x_{k+1} = \mu x_n (1 - x_n) \tag{39}$$

The Logistic is in the chaotic state when $x \in (0, 1)$ and $\mu = 4$. FIG. 4. shows the probability distribution of range (0, 1) obtained by iterating the Logistic mapping for 100000 times.

As can be seen from FIG. 4, the high probability distribution at the two ends of Logistic chaos sequence has limitations reducing the algorithm efficiency. Skew Tent chaotic sequence has the advantages of equal probability density and less searching time, but there are disadvantages such as unstable periodic points and so on. Therefore, combining it with the Logistic chaos sequence effectively solves this problem, and the mathematical expression obtained is:

$$\begin{cases} x_{k+1} = x_k / \varphi_k \quad 0 < x_k < \varphi_k \\ x_{k+1} = (1 - x_k)/(1 - \varphi_k) \quad \varphi_k < x_k < 1 \end{cases} \tag{40}$$

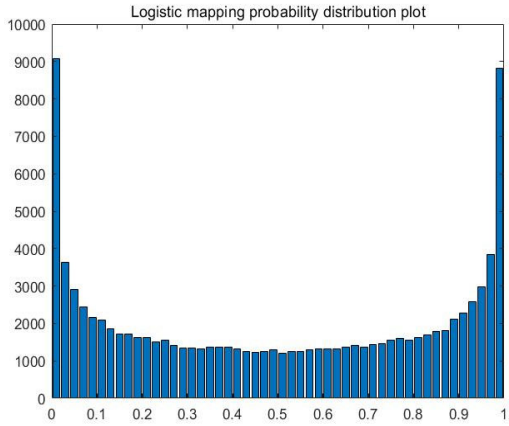

FIGURE 4. Logistic mapping probability distribution.

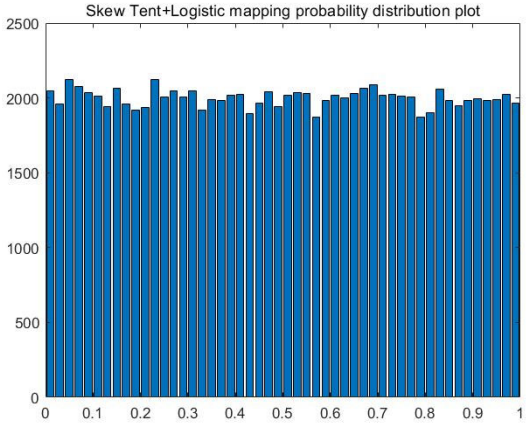

FIGURE 5. Probability distribution of Skew Tent combining with Logistic mapping.

where φ_k is subject to the Logistic mapping. With the combination used in this paper, the probability distribution for 100000 iterations is presented in FIG. 5.

It can be seen from FIG. 5 that the combination of chaotic sequences has a uniform distribution of probability density functions, which effectively solves the problem of failing to extract information accurately due to local search, and reduces the impact of selection for initial values on global search ability.

In WOA, the phenomenon of unchanged leader $X^*(t)$ position after multiple iterations causes early convergence, i.e., the rapid convergence to the local optimum when solving the optimization problem, which ultimately degrades the quality of algorithm solutions.

C. WOA BASED ON CROSS OPERATORS WITH GAUSSIAN VARIATIONAL OPERATORS

Aiming at addressing the above problems, this paper combines the prey position with the crossover operators and Gaussian variational operators of the genetic algorithm, making the algorithm jump out of local optimum rapidly.

$$\begin{cases} A^k = \alpha^* A^{k+1} + (1-\alpha)^* A^k \\ A^{k+1} = \alpha^* A^k + (1-\alpha)^* A^{k+1} \end{cases} \tag{41}$$

where A^k denotes the position of optimal prey in k generation population; A^{k+1} indicates the position of other random preys in k generation population; and α is the random crossover operator.

The prey individuals of new generations are mainly determined by α and individuals of previous generations. When α converges to 0.5, the offspring moves away from father, which can expand the searching space and ensure the population diversity; when α moves away from 0.5, the offspring moves closer to father, which narrows the searching range and improves the searching accuracy. The expression of improved crossover operator is:

$$\alpha = \min(\alpha) + (\max(\alpha) - \min(\alpha)) * e^{\frac{T}{T}} \tag{42}$$

where $\min(\alpha)$ and $\max(\alpha)$ represent the minimum and maximum values of α, respectively; and T is the maximum number of iterations.

To ensure that the gene proportion of A^k and A^{k+1} in the offspring is more balanced at the beginning of iteration, the initial value of α is set as 0.5, which rapidly approaches 1 as the iteration number grows, making the search accuracy increase.

The variation operator prevents the algorithm from falling into a local optimum, while also maintaining the population diversity. In addition, with the aim of reducing the probability for prematureness and falling into the local optimum in conventional WOA, this paper performs the Gaussian variational operation on the current optimal solution with following expression:

$$X_{best}(t+1) = X_\alpha(t)(1 + Gaussion(\sigma)) \tag{43}$$

where $X_{best}(t+1)$ refers to the position of individual after variation; $Gaussion(\sigma)$ is a random variable subjecting to the Gaussian distribution. The global optimal position is updated as follows:

$$X_\alpha(t+1) = \begin{cases} X_{best}(t+1), \text{others} \\ X_\alpha(t), f(X_{best}(t+1)) > f(X_\alpha(t)) \\ \text{and } rand_4 < p \end{cases} \tag{44}$$

where $rand_4$ indicates the random variable in interval [0, 1]; p represents the selection probability; and $f(\cdot)$ is the fitness value of individual. From Eq. (23), it can be seen that falling into the local optimum can be avoided through performing the mutation operation on the current global optimum solution $X_\alpha(t)$.

In conclusion, the flow chart of IWOA proposed in this paper is shown in FIG. 6.

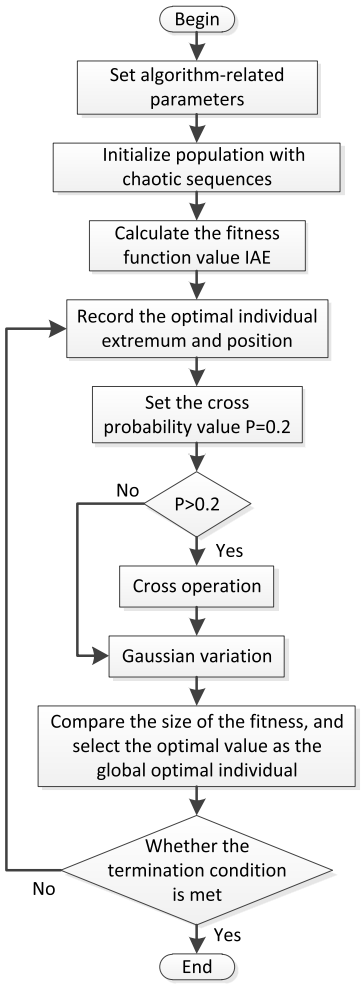

FIGURE 6. Flow chart of IWOA.

D. COMPLEXITY ANALYSIS OF THE IWOA ALGORITHM

The time complexity can be used as one of the criteria to judge the performance of an algorithm, which reflects the operational efficiency of the algorithm. In the WOA algorithm, the population size is assumed to be N and the individual dimension is n. Since the search ability and solution accuracy of algorithm do not only depend on the evolutionary algebra and population size, the basic variable that determines the time complexity of an algorithm when solving a problem is the dimension of the individual space representing the problem magnitude.

In the initialization phase of the algorithm, suppose that: t_1 is the time to set the value and position of the optimal individual objective function, and t_2 is the time to set each dimensional vector of individual, then the time complexity of this process is:

$$T_1 = O(t_1 + N \cdot (n \cdot t_2)) = O(n) \tag{45}$$

The total number of cycles to enter the loop is $T_{\max}$. Let: the time to perform the out-of-bounds wording for each dimension of the individual be t_3, the time to solve the objective function be $f(n)$, the time to update the best individual be t_4, and the time to update the coefficient A and C vectors by Eqs. (32) and (33) be t_5 and t_6, respectively. The time complexity of this process is:

$$T_2 = O(N \cdot (n \cdot t_3 + f(n) + t_4 + t_5 + t_6)) = O(n + f(n)) \tag{46}$$

Suppose that there are m_1 individuals in the population which are searching for food at random, m_2 individuals are narrowing down to surround food, and m_3 individuals are feeding in a spiral bubble net ($N = m_1 + m_2 + m_3, 0 \leq m_1, m_2, m_3 \leq N$), and that the time to update each dimensional vector by Eqs. (31) and (36) when each individual is executing one of these three different strategies are t_7, t_8 and t_9, respectively. The time complexity of this process is:

$$T = T_1 + T_{\max} \cdot (T_2 + T_3) = O(n + f(n)) \tag{47}$$

In IWOA, the population size is N, the dimension of each individual is n, the population position is initialized using two chaotic mappings, and the complexity of this time is: $O(N)$. During the iteration, the total number of iterations is set to $T_{\max}$, the number of crossover operator iterations is T_c, the time complexity of calculating the variation judgment factor and updating the population position after variation is $O(T_{\max} \cdot (\frac{N}{2} + 1))$, and the time complexity of calculating the random crossover operator complexity is $O(T_c)$.

From the above analysis, it can be seen that the time complexity of IWOA is the sum of the WOA time complexity and the above three-time complexities, and the result does not change the order of magnitude of the time complexity, so the IWOA proposed in this paper does not reduce the operational efficiency of the algorithm.

E. IWOA PERFORMANCE TESTING

In this section, we use typical test functions F1, F2, F3, and F4 to evaluate the convergence speed, local and global search capability, and convergence accuracy of the IWOA, which are shown in Table 3. In order to provide a more intuitive representation of the IWOA search performance, the experimental results are compared with those of the conventional WOA, PSO, GA and MFO algorithms. In order to ensure the fairness of the experiments, the four algorithms are independently tested 50 times and all the experimental results are de-averaged (Ave), minimized (Min) and standard deviated (Std) with a population size of 100 and iterations of 100. The specific experimental results are shown in Table 4, where the optimal solutions are shown in bolded font. The corresponding plots of the test functions in three-dimensional space and the positions of convergence to the optimal values are shown in FIGs. 7-10.

As can be seen from Table 4, for the single-peaked test functions F1 and F2, Ave and Min of IWOA proposed in this paper are the smallest, which indicates that the global convergence accuracy and optimization finding ability of IWOA are better than other three algorithms. For the multi-peak test functions F3 and F4, Ave and Min of IWOA proposed in this

TABLE 3. List of test functions.

Function	Expression	Value range
F1	$f_1(x_i)=\sum_{i=1}^{30}x_i^2$	[−100,100]
F2	$f_2(x_i)=\sum_{i=1}^{30}\lvert x_i\rvert+\prod_{i=1}^{30}\lvert x_i\rvert$	[−100,100]
F3	$f_3(x_i)=\sum_{i=1}^{30}[x_i^2-10\cos(2\pi x_i)+10]$	[−5.12,5.12]
F4	$f_4(x_i)=-20\exp(-0.2\sqrt{\frac{1}{30}\sum_{i=1}^{30}x_i^2})-\exp(\frac{1}{30}\sum_{i=1}^{30}\cos(2\pi x_i))+20+e$	[−32,32]

TABLE 4. Test result.

function	category	IWOA	WOA	PSO	MFO	GA
F1	Min	1.69E-44	2.72E-21	1.17E+04	7.36E+02	1.40E-01
	Ave	1.94E-27	2.25E-17	2.03E+04	3.09E+03	3.40E-01
	Std	9.72E-27	7.08E-17	3.49E+03	2.50E+03	1.63E-01
F2	Min	4.29E-25	1.17E-13	8.97E-01	1.14E+01	1.31E+00
	Ave	1.33E-17	4.17E-11	2.40E+00	3.38E+01	2.21E+00
	Std	4.11E-17	6.91E-11	9.21E-01	1.40E+01	3.88E-01
F3	Min	0.00E+00	0.00E+00	9.14E+00	1.02E+02	1.68E+01
	Ave	0.00E+00	2.83E-01	2.67E+01	1.75E+02	2.65E+01
	Std	0.00E+00	2.02E+00	8.17E+00	3.20E+01	8.17E+00
F4	Min	8.88E-16	5.96E-12	2.05E+00	6.98E+00	3.08E-01
	Ave	2.88E-15	7.77E-10	3.23E+00	1.16E+01	7.54E-01
	Std	3.67E-15	1.14E-09	5.77E-01	1.95E+00	1.76E-01

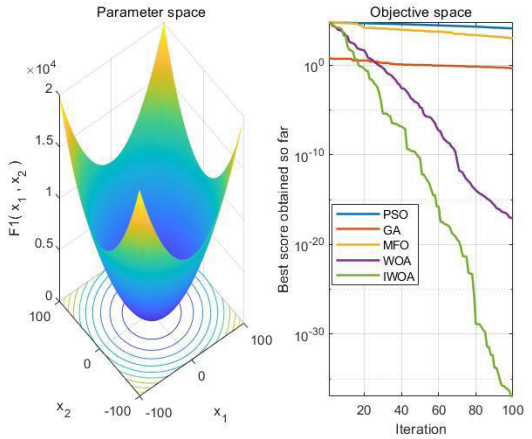

FIGURE 7. Test function F1.

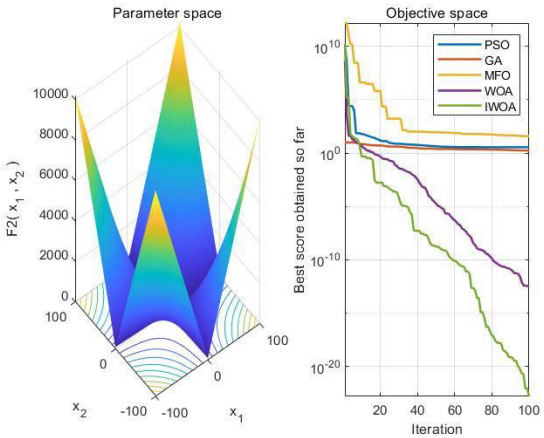

FIGURE 8. Test function F2.

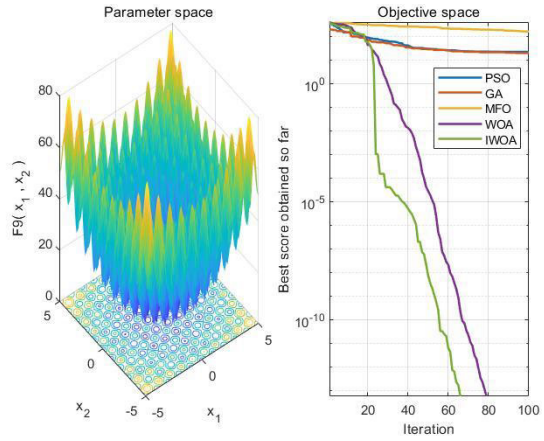

FIGURE 9. Test function F3.

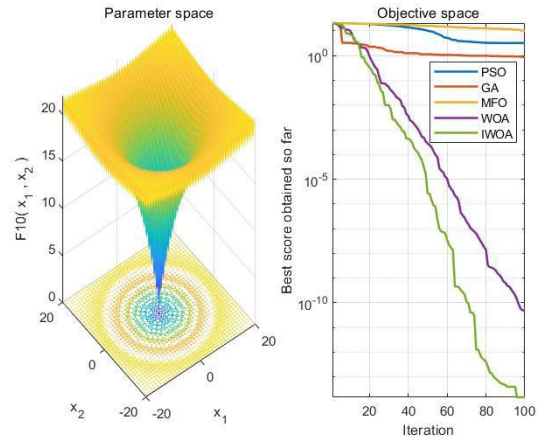

FIGURE 10. Test function F4.

paper are also smaller than those of the other algorithms, indicating that the IWOA has better local optimization capability than the other algorithms. For all the test functions, Std of the solutions of IWOA is the smallest compared with other algorithms, which indicates that the stability of it is stronger than other algorithms. As the number of solution dimensions increases, Std of IWOA does not change significantly, which indicates that it has better accuracy and stability in solving complex non-linear mathematical models.

V. SIMULATION TESTS AND ANALYSIS

Based on the principles described above, the corresponding simulation model is constructed in Matlab/Simulink in this paper to obtain the tracking and error effects of the ADRC controller, the PID controller and the proposed IWOA-Fuzzy-ADRC controller on the position attitude of the quadrotor UAV. In addition, to demonstrate the superiority of IWOA-Fuzzy-ADRC controller, it is compared with PID and ADRC algorithms in terms of dynamic response and steady-state accuracy in this paper.

A. OPTIMIZATION AND ASSIGNMENT OF SIMULATION PARAMETERS

In this paper, the IWOA algorithm is employed to optimize $kbetai\_x(i = 1, 2)$, $kbeta0i\_x(i = 1, 2, 3)$, β_1, β_2, and $\beta_{0i}(i = 1, 2, 3)$ of the fuzzy ADRC controller for faster and more accurate quadrotor UAV position trajectory tracking with less tracking error. With the number of iterations at 200, taking the position control as y direction, the parameter iteration curves for the optimal adjustment factor and the quantization factor to adjust the input range of fuzzy controller are shown in FIG. 11. In the case of attitude controller *pitch*, the parameter curves for the calculus gains β_1 and β_2 of Fuzzy-NLSEF, as well as the output error gain $\beta_{0i}(i = 1, 2, 3)$ of Fuzzy-ESO are shown in FIG. 12.

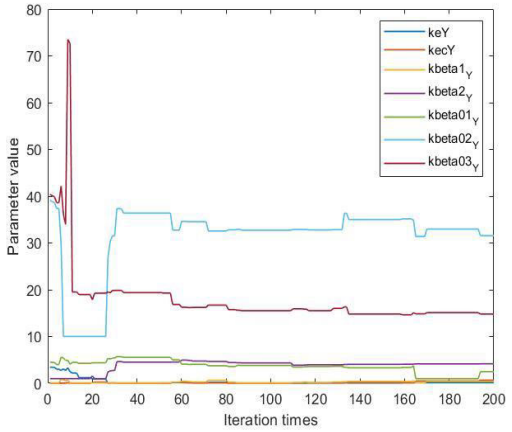

FIGURE 11. Iteration curves for optimal adjustment coefficient and quantization factor of position *y* direction fuzzy controller.

As can be seen from FIGs. 11-12, the IWOA, optimized by the two chaotic mappings, the crossover operators and the Gaussian variant, enables controller parameters to converge faster and without easily falling into local optima.

The values of required parameters for the fuzzy ADRC position controller and the attitude controller are listed in Tables 5-6, respectively.

B. ANALYSIS OF SIMULATION RESULTS

FIG. 13 illustrates the convergence curve of IWOA fitness function for iteration number 200 and population size 100. It can be seen that the trend of curve decreases and then converges to a stable state. When the iteration number is 30, the

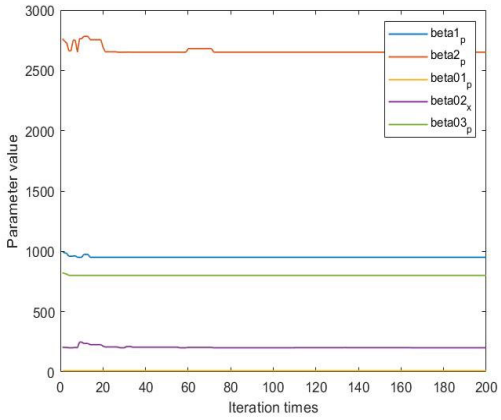

FIGURE 12. Parameters setting curves of attitude controller *pitch* channel.

TABLE 5. Position controller parameters of the ADRC algorithm.

Position	TD	ESO
X	$h_0 = 0.01$ $r = 300$	$\alpha_1 = 0.75, \alpha_2 = 0.5, \alpha_3 = 0.25$ $\delta = 2$
Y	$h_0 = 0.01$ $r = 300$	$\alpha_1 = 0.75, \alpha_2 = 0.5, \alpha_3 = 0.25$ $\delta = 2$
Z	$h_0 = 0.01$ $r = 180$	$\alpha_1 = 0.75, \alpha_2 = 0.5, \alpha_3 = 0.25$ $\delta = 3$

TABLE 6. Attitude controller parameters of the ADRC algorithm.

Attitude	TD	ESO
ϕ	$h_0 = 0.01$ $r = 180$	$\alpha_1 = 0.75, \alpha_2 = 0.5, \alpha_3 = 0.25$ $\delta = 3$
θ	$h_0 = 0.01$ $r = 180$	$\alpha_1 = 0.75, \alpha_2 = 0.5, \alpha_3 = 0.25$ $\delta = 3$
ψ	$h_0 = 0.008$ $r = 100$	$\alpha_1 = 0.75, \alpha_2 = 0.5, \alpha_3 = 0.25$ $\delta = 5$

fitness value of IWOA converge to be stable and the fitness value of IWOA is low, indicating that the solution searched by IWOA is of high quality, i.e., the search performance, convergence speed and accuracy of the algorithm achieve satisfactory results.

FIGs. 14-16 presents the tracking comparison curves of the position trajectory for the IWOA-Fuzzy-ADRC controller, the ADRC controller and the PID controller in quadrotor UAV under the position x, y and z directions, where x_d, y_d and z_d are the position expectation values.

From FIG. 14, it can be seen that in direction, the IWOA-Fuzzy-ADRC controller can track the desired trajectory in real time within 3.15s, while the ADRC and PID take 4.97s and 5.05s respectively to fully track the desired trajectory. Additionally, the ADRC controller and PID controller have the problems of steady-state error and large overshoot, resulting the control performances of them are far inferior to that of the IWOA-ADRC controller. In the same way, as shown

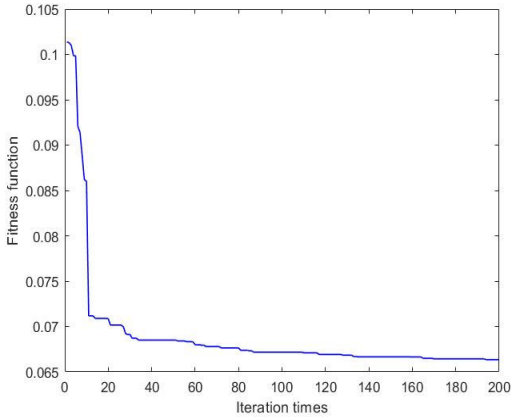

FIGURE 13. Convergence curve of fitness function.

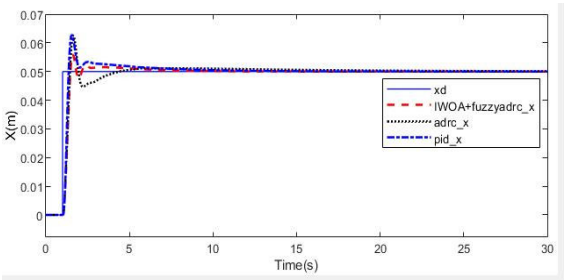

FIGURE 14. Curve of position trajectory tracking in x direction.

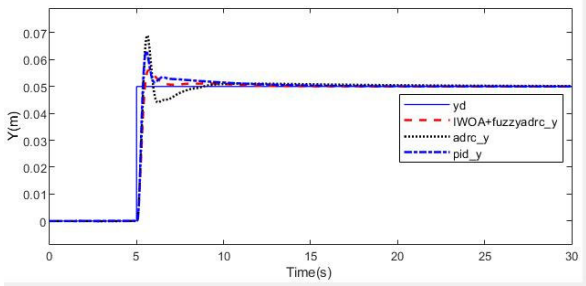

FIGURE 15. Curve of position trajectory tracking in y direction.

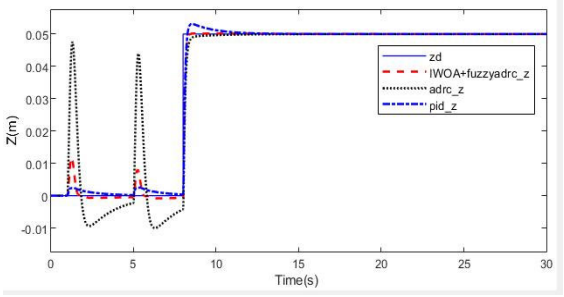

FIGURE 16. Curve of position trajectory tracking in z direction.

in FIGs. 15-16, the IWOA-Fuzzy-ADRC controller in y and z direction outperforms both ADRC and PID in terms of steady-state accuracy as well as dynamic performance.

The comparative real-time position tracking error curves of the IWOA-Fuzzy-ADRC controller, the ADRC controller and the PID controller for the quadrotor UAV in x, y and z

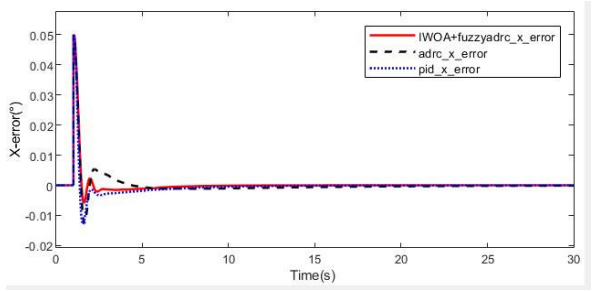

FIGURE 17. Curve of position error tracking in x direction.

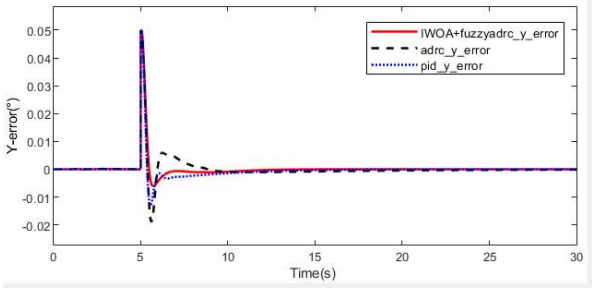

FIGURE 18. Curve of position trajectory tracking in y direction.

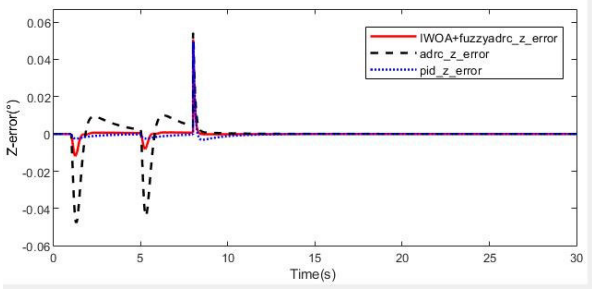

FIGURE 19. Curve of position trajectory tracking in z direction.

directions are shown in FIGs. 17-19. We can observe that the IWOA-Fuzzy-ADRC controller converges at relatively rapid rate in three directions, while the errors of the ADRC and PID converge at relatively slow rate. As a result, it can be concluded that the controller designed in this paper is able to accurately and quickly track the desired position trajectory in real time, effectively improve the dynamic performance of system as well as the steady-state accuracy.

The results of calculating various performance metrics for IWOA-Fuzzy-ADRC controller, ADRC controller and PID controller real-time tracking position trajectories in x and y directions are shown in Tables 7-8. It can be seen that the IWOA-Fuzzy-ADRC controller outperforms the ADRC and PID in terms of dynamic performance and steady-state accuracy.

The comparative real-time trajectory tracking curves and real-time trajectory tracking error curves for IWOA-Fuzzy-ADRC controller, ADRC controller and PID controller of quadrotor UAV with Roll channel attitude angle *roll* are shown in FIGs. 20-21, and pitch channel attitude angle *pitch* are shown in FIGs. 22-23. It can be seen that the IWOA-Fuzzy-ADRC controller tracks the attitude angle in the fastest

TABLE 7. Performance metrics of position tracking in *x* direction.

x	Overshoot /（%）	Steady state error /（°）	Interference regulation time /s
IWOA-Fuzzy-ADRC	11.66	$1.29*10^{-19}$	4.23
ADRC	24.44	$1.11*10^{-4}$	9.23
PID	25.85	$4.10*10^{-7}$	6.27

TABLE 8. Performance metrics of position tracking in *y* direction.

y	Overshoot /（%）	Steady state error /（°）	Interference regulation time /s
IWOA-Fuzzy-ADRC	12.07	$1.09*10^{-9}$	4.76
ADRC	37.63	$1.48*10^{-4}$	7.13
PID	25.90	$1.57*10^{-6}$	6.33

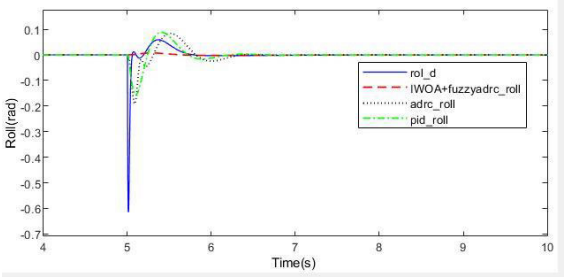

FIGURE 20. Tracking curve of rolling angle trajectory.

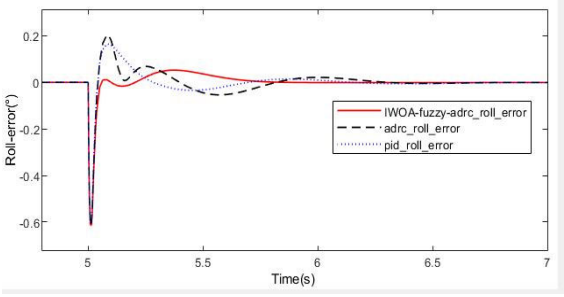

FIGURE 21. Trajectory error curve of roll angle tracking.

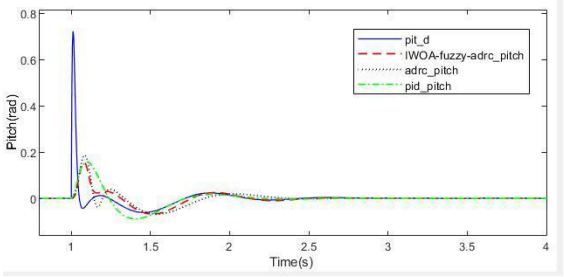

FIGURE 22. Tracking curve of pitching angle trajectory.

and best way, and its tracking error converges the most rapidly, indicating that the IWOA-Fuzzy-ADRC controller can effectively restrain interference, ensure the system stability, and track the attitude in real time accurately. Whereas the ADRC and PID have a slower error convergence rate,

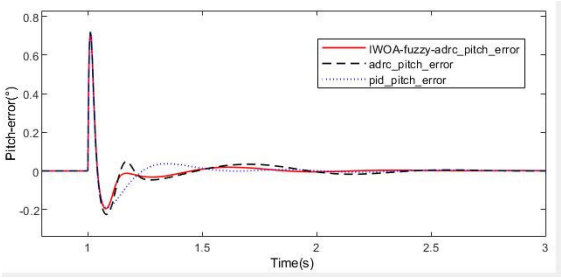

FIGURE 23. Trajectory error curve of pitch angle tracking.

which indicates that both cannot get good results for tracking complex trajectories.

The above experimental results demonstrate that the IWOA-Fuzzy-ADRC controller designed in this paper can ensure excellent results in tracking complex trajectories of quadrotor UAV, making it converge rapidly and steadily to the desired trajectory, and rendering the control system have better dynamic response and steady-state accuracy.

VI. CONCLUSION

In order to provide fast and accurate tracking for the position and attitude trajectory of a quadrotor UAV, an IWOA-Fuzzy-ADRC controller has been designed in this paper. The specific works are as follows: (1) The initial population diversity of WOA has been improved by combining logistic chaos mapping and skew tent mapping, which has solved the problem of low convergence accuracy and slow speed of traditional WOA. (2) The global search capability of WOA has been enhanced by introducing the crossover operator and Gaussian variational operator, which prevent it from falling into local optimum. (3) IWOA has been obtained by combining (1) and (2) as well as optimizing the optimal adjustment coefficients of the fuzzy self-adjoint controller, the calculus gain of NLSEF and the error correction coefficients of ESO. The simulation results show that the proposed method can improve the tracking effect of the position and attitude for quadrotor UAV more effectively than some traditional methods, with faster response time, higher steady-state accuracy and stronger robustness to external disturbances. Taking x-direction position trajectory tracking as an example, the controller can reduce overshoot to 47.7% and adjustment time to 45.8% compared to conventional ADRC, and overshoot to 45.1% and adjustment time to 67.5% compared to conventional PID. The controller can reduce the overshoot to 32% and the adjustment time to 66.8% in y-direction position trajectory tracking compared to conventional ADRC, and reduce the overshoot to 46.7% and the adjustment time to 75.2% compared to conventional PID. This effectively reduces the adjustment time and magnitude of the UAV attitude trajectory tracking.

To address the shortcomings of this paper, in future research, we will use other fuzzy control techniques in the design of this controller, such as IT2FLC [27], to investigate the effectiveness of the controller for UAV attitude trajectory tracking. In addition, to demonstrate the practicality of

the controller and the comprehensiveness of the application scenarios, we will analyze the attitude trajectory tracking of fixed-rotor UAV and multi-rotor UAV [28], [29].

REFERENCES

[1] J. Dou, X. Kong, and B. Wen, "Altitude and attitude active disturbance rejection controller design of a quadrotor unmanned aerial vehicle," *Proc. Inst. Mech. Eng., G, J. Aerosp. Eng.*, vol. 231, no. 9, pp. 1732–1745, Jul. 2017.
[2] L. Xu, H. Ma, D. Guo, A. Xie, and D. Song, "Backstepping sliding-mode and cascade active disturbance rejection control for a quadrotor UAV," *IEEE/ASME Trans. Mechatronics*, vol. 25, no. 6, pp. 2743–2753, Dec. 2020.
[3] Q. Han, "Active disturbance rejection control technology," *Frontiers Sci.*, vol. 1, pp. 24–31, Jun. 2007.
[4] L. Wang, "Research on control technology of four-rotor unmanned aerial vehicle," M.S. thesis, Dept. Automat., Harbin Eng Univ., Harbin, China, 2012.
[5] W. R. Abdul-Adheem, I. K. Ibraheem, A. J. Humaidi, and A. T. Azar, "Model-free active input–output feedback linearization of a single-link flexible joint manipulator: An improved active disturbance rejection control approach," *Meas. Control*, vol. 54, nos. 5–6, pp. 856–871, May 2021.
[6] A. J. Humaidi and H. M. Badr, "Linear and nonlinear active disturbance rejection controllers for single–link flexible joint robot manipulator based on PSO tuner," *J. Eng. Sci. Technol. Rev.*, vol. 11, no. 3, pp. 133–138, Apr. 2018.
[7] W. Ning, L. Zhe, L. Xiaolong, and Z. Jiaqiang, "Design of UAV yaw angle controller based on variable domain fuzzy PID," *J. Phys., Conf.*, vol. 1754, no. 1, Feb. 2021, Art. no. 012112.
[8] S. Xu, Z. Wu, and Y. Ni, "Adaptive fuzzy active disturbance rejection control for variable load quadrotor UAV," *Transducer Microsyst.*, vol. 41, no. 7, pp. 101–105, 2022.
[9] H. Sun, Q. Liu, A. Liu, L. Feng, and H. Wu, "An industrial quadrotor UAV control method based on fuzzy adaptive linear active disturbance rejection control," *Electronics*, vol. 10, no. 4, p. 376, 2021.
[10] L. Tao, Q. Chen, Y. Nan, F. Dong, and Y. Jin, "Speed tracking and synchronization of a multimotor system based on fuzzy ADRC and enhanced adjacent coupling scheme," *Complexity*, vol. 2018, pp. 1–16, Sep. 2018.
[11] B. Gao, H. Guan, W. Shen, and Y. Ye, "Application of the gray wolf optimization algorithm in active disturbance rejection control parameter tuning of an electro-hydraulic servo unit," *Machines*, vol. 10, no. 8, p. 599, Jul. 2022.
[12] J. Ren, Z. Chen, Y. Yang, M. Sun, Q. Sun, and Z. Wang, "Grey wolf optimization based active disturbance rejection control parameter tuning for ship course," *Int. J. Control, Autom. Syst.*, vol. 20, no. 3, pp. 842–856, Mar. 2022.
[13] C. Li, "Adaptive active disturbance rejection control of servo system based on RBF neural network," *Elect. Automat.*, vol. 32, no. 2, pp. 23–25, 2010.
[14] J. P. B. Araque, A. Zavoli, D. Trotta, and G. De Matteis, "Genetic algorithm based parameter tuning for robust control of launch vehicle in atmospheric flight," *IEEE Access*, vol. 9, pp. 108175–108189, 2021.
[15] S. Yun, H.-S. Lee, J. Woo, S.-H. Byun, I. Choi, J. Lee, and I.-Y. Seo, "PID control parameters tuning technique of power plant based on genetic algorithm for multivariable control performance optimization," *Trans. Korean Inst. Electr. Eng.*, vol. 69, no. 1, pp. 1–8, Jan. 2020.
[16] Y. Zhou, H. Gao, B. Zhao, and L. Zhao, "A GA based parameters tuning method for an ADRC controller of ISP for aerial remote sensing applications," *ISA Trans.*, vol. 81, pp. 318–328, Oct. 2018.
[17] C. Xi, W. Dejin, and L. Fasong, "PH control via internal circulation foam floatation tower based on online self-adaption genetic algorithm-PID parameters setting," *J. Comput. Theor. Nanoscience*, vol. 13, no. 12, pp. 9363–9367, Dec. 2016.
[18] M. Liu, R. Lin, M. Yang, A. V. Nazarova, and J. Huo, "Active disturbance rejection motion control of spherical robot with parameter tuning," *Ind. Robot, Int. J. Robot. Res. Appl.*, vol. 49, no. 2, pp. 332–343, Feb. 2022.
[19] X.-J. Wang, Y.-M. Feng, and Y.-W. Sun, "Research on improved active disturbance rejection control of continuous rotary motor electro-hydraulic servo system," *J. Central South Univ.*, vol. 27, no. 12, pp. 3733–3743, Dec. 2020.
[20] Y. Shen and F. Xu, "Adaptive neural network based active disturbance rejection flight control of an unmanned helicopter," *Aerosp. Sci. Technol.*, vol. 119, Dec. 2021, Art. no. 107062.
[21] G. Xu, Q. Wang, X Guo, and J. Xing, "Review of whale optimization algorithms," *Appl. Res. Comput.*, vol. 40, no. 2, pp. 328–336, 2023.
[22] Z. Cui, H. Zeng, B. Huang, J. Liu, and Y. Wei, "Optimization of control parameters of bidirectional LLC resonant converter based on whale optimization algorithm," *Manuf. Automat.*, vol. 43, no. 9, pp. 83–86, 2021.
[23] H. Li, "Research on control system of four-rotor UAV based on active disturbance rejection algorithm," M.S. thesis, Dept. Mech. Eng., Chongqing Univ., Chongqing, China, 2020.
[24] W. Wei, Y. Wu, F. Li, F. Wang, and Z. Zhang, "Trajectory tracking control of four-rotor UAV based on improved active disturbance rejection," *New Technol. Electroeng. Electr. Energy*, vol. 42, no. 5, pp. 1–13, 2023.
[25] K. C. Sio and C. K. Lee, "Stability of fuzzy PID controllers," *IEEE Trans. Syst., Man, Cybern. A, Syst. Humans*, vol. 28, no. 4, pp. 490–495, Jul. 1998.
[26] F. Wang, H. Liao, H. Liang, and W. Sun, "An improved whale optimization algorithm based on siege mechanism," *Control Decis.*, vol. 37, pp. 1–9, Jun. 2023.
[27] A. J. Humaidi, H. T. Najem, A. Q. Al-Dujaili, D. A. Pereira, I. K. Ibraheem, and A. T. Azar, "Social spider optimization algorithm for tuning parameters in PD-like interval type-2 fuzzy logic controller applied to a parallel robot," *Meas. Control*, vol. 54, nos. 3–4, pp. 303–323, Mar. 2021.
[28] Z. Ren, S. Xu, Y. Su, and D. Chen, "An active disturbance rejection attitude controller for multi-rotor UAV," *Mod. Comput.*, vol. 28, no. 8, pp. 93–99, 2022.
[29] L. Fei, N. Li, and Y. Li, "Active disturbance rejection reverse step control of fixed wing UAV," *Control Theory Appl.*, vol. 33, no. 10, pp. 1296–1302, 2016.

ZEBIAO SHAN received the Ph.D. degree from Jilin University, in 2016. He is currently a Lecturer and a Master Supervisor with the Changchun University of Science and Technology and a Postdoctoral Fellow with the Changchun Institute of Meteorological Instruments and Jilin University. His research interests include weak signal detection, array signal processing, and robot control technology.

YUHANG WANG received the bachelor's degree from Northeast Petroleum University, in 2020. He is currently pursuing the master's degree with the Changchun University of Science and Technology, Jilin, China. His current research interests include UAV position trajectory tracking, control, and optimization algorithms.

XIAOSONG LIU received the Ph.D. degree from Jilin University, in 2016. She is currently a Lecturer and a Master Supervisor with the Changchun University of Science and Technology. Her research interests include information perception and advanced control technology, modeling, simulation, and the control of complex systems.

CHANGBIN WEI received the bachelor's degree from Dezhou University, in 2021. He is currently pursuing the master's degree with the Changchun University of Science and Technology, Jilin, China. His current research interests include unmanned vehicle trajectory tracking and control and active disturbance rejection control algorithm.